Nanoscale

Low-threshold Laser Medium Utilizing Semiconductor Nanoshell Quantum Dots

Journal:	*Nanoscale*
Manuscript ID	NR-ART-05-2020-003582.R1
Article Type:	Paper
Date Submitted by the Author:	23-Jul-2020
Complete List of Authors:	Porotnikov, Dmitry; BGSU, Department of Chemistry Diroll, Benjamin; Argonne National Laboratory, Center for Nanoscale Materials Harankahage, Dulanjan; BGSU, Department of Physics and Astronomy Obloy, Laura; BGSU, Department of Chemistry Yang, Mingrui; BGSU Cassidy, James; BGSU Ellison, Cole; BGSU Miller, Emily; BGSU Rogers, Spencer; University of Rochester Tarnovsky, Alexander; BGSU, Department of Chemistry Schaller, Richard; Northwestern University; Argonne National Laboratory, Center for Nanoscale Materials Zamkov, Mikhail; BGSU

Low-threshold Laser Medium Utilizing Semiconductor Nanoshell Quantum Dots.

Dmitry Porotnikov,[1,2] Benjamin T. Diroll,[6] Dulanjan Harankahage,[1,2] Laura Obloy[1,3], Mingrui Yang,[1,2] James Cassidy,[1,2] Cole Ellison[1,2], Emily Miller,[1,2] Spencer Rogers,[5] Alexander N. Tarnovsky,[1,3] Richard D. Schaller,[4,6] Mikhail Zamkov.[1,2]

The Center for Photochemical Sciences[1], Department of Physics[2] and Department of Chemistry[3], Bowling Green State University, Bowling Green, Ohio 43403. Department of Chemistry[4], Northwestern University, Evanston, Illinois 60208. Department of Physics and Astronomy[5], University of Rochester, Rochester, New York 14627. Center for Nanoscale Materials[6], Argonne National Laboratory, Lemont, Illinois 60439.

Corresponding author: zamkovm@bgsu.edu; Tel: 419-372-0264; Fax: 419-372-9938

Keywords: Optical gain, nanoplatelets, stimulated, biexcitons, catalysis.

Abstract. Colloidal semiconductor nanocrystals (NCs) represent a promising class of nanomaterials for lasing applications. Currently, one of the key challenges facing the development of high-performance NC optical gain media lies in enhancing the lifetime of biexciton populations. This usually requires the employment of charge-delocalizing particle architectures, such as core/shell NCs, nanorods, and nanoplatelets. Here, we report on a two-dimensional nanoshell quantum dot (QD) morphology that enables a strong delocalization of photoinduced charges,

leading to enhanced biexciton lifetimes and low lasing thresholds. A unique combination of a large exciton volume and a smoothed potential gradient across interfaces of the reported CdS_{bulk}/CdSe/CdS_{shell} (core/shell/shell) nanoshell QDs results in strong suppression of Auger processes, which was manifested in this work though the observation of stable amplified stimulated emission (ASE) at low pump fluences. An extensive charge delocalization in nanoshell QDs was confirmed by transient absorption measurements, showing that the presence of a bulk-size core in CdS_{bulk}/CdSe/CdS_{shell} QDs reduces exciton-exciton interactions. Overall, present findings demonstrate unique advantages of the nanoshell QD architecture as a promising optical gain medium in solid-state lighting and lasing applications.

1. Introduction

The development of colloidal quantum dot lasers has received considerable attention in the past two decades.[1-3] Compared to traditional, epitaxial quantum-well lasers,[4-6] colloidal nanocrystal (NC) devices show promise for further reduction of lasing thresholds,[7-8] a spectrally narrower emission,[9] and a wider range of spectral tunability.[10-12] Potential benefits are also expected from the device fabrication standpoint, as the synthesis of colloidal NCs relies on low-cost chemical techniques,[9] which alleviates the need for complex epitaxial deposition methods. Such chemically fabricated and scalable nanoparticle inks can be solution-processed onto various substrates providing compatibility with a variety of laser cavity types and geometries.[13] Over the last decade, several successful demonstrations of chalcogenide and halide perovskite[14,15] QD-based lasing media have appeared in literature, including recent reports of continuous-wave, room temperature CdSe nanoplatelet lasers[16-18] operating at low input powers of 1 μW.[17]

The advent of colloidal QD lasers has been largely motivated by the unique properties of quantum-confined semiconductors, which can support a tunable, temperature-insensitive optical gain.[8,19,20] Unfortunately, the presence of strong carrier confinement in colloidal NCs has also been

associated with issues that impeded the progress of QD-based gain media. As demonstrated by early investigations,[21,22] enhanced Coulomb interactions in quantum-confined semiconductors greatly increase the rate of multi-exciton Auger decay, leading to high thresholds for the amplified stimulated emission (ASE). This issue was particularly evident in the case of zero-dimensional (0D) NCs, where strong carrier confinement in all three spatial dimensions prevented the onset of ASE.[1,23] In light of these limitations, QD lasers have been exclusively employing low-dimensional nanoscale geometries exhibiting a reduced electron–hole overlap. These included giant core/shell QDs,[24] alloyed core/shell QDs,[25] 1D nanorods,[26-28] tetrapods,[29] and 2D nanoplatelets.[16,30,32,33] The spatial delocalization of photoinduced charges in these nanostructures has been credited for the increase of corresponding multi-exciton lifetimes by 10-100 times relative to 0-D NCs, ultimately leading to lower ASE thresholds and high modal gains. Recently, synthetic methods have been developed for the growth of 2D quantum wells utilizing a spherical-shell geometry.[34-36] These, so-called nanoshell QDs, featuring a CdS_{bulk}/CdSe/CdS_{shell} core/shell/shell morphology **(Figs. 1a, 1b)**, can effectively suppress Auger recombination processes due to a large volume of a spherical CdSe quantum well, making a strong case for the development of nanoshell-based optical gain media.[36] Previously, however, the emission quantum yield of nanoshell QDs had been too low compared to other charge-delocalizing semiconductor morphologies,[36] precluding their deployment as active laser media.

Here, we demonstrate that CdS_{bulk}/CdSe/CdS_{shell} nanoshell QDs comprising a CdSe quantum-well layer represent a promising nanoscale morphology for the development of lasing applications. The presence of the bulk-size core domain in these nanostructures allows manipulating the diameter of the CdSe quantum-confined shell while maintaining approximately the same degree of quantum confinement in the radial dimension. Thus, for the same given surface

area as in the case of zero-, one-, or other two-dimensional geometries, nanoshell QDs exhibit the largest effective biexciton volume **(**Fig. SF1b**)**, which makes these materials particularly suitable for achieving Auger suppression. In the course of this work, we have carefully balanced the dimensions of the three domains in $CdS_{bulk}/CdSe/CdS_{shell}$ nanoshell QDs towards enhancing both single- and bi-exciton lifetimes. The resulting nanoshells were processed into solids exhibiting the onset of the amplified stimulated emission at low pump fluences. A combination of ultrafast transient absorption and time-resolved photoluminescence measurements have attributed such promising optical gain performance to strong suppression of Auger processes, which provided little competition to ASE.

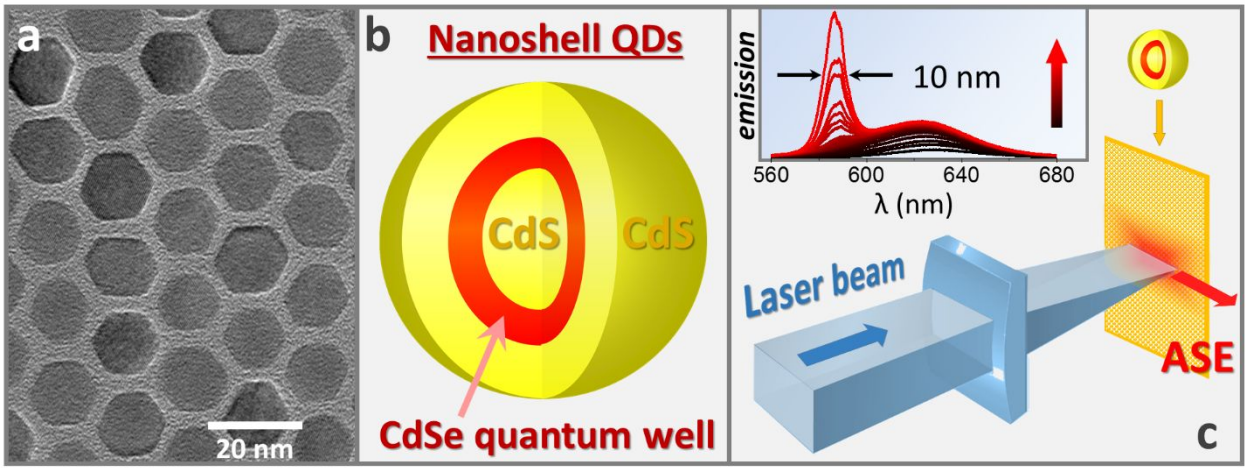

Figure 1. (a). Transmission Electron Microscope (TEM) image of ~16-nm $CdS_{bulk}/CdSe/CdS_{shell}$ nanoshell QDs. (b). Schematic illustration of a $CdS_{bulk}/CdSe/CdS_{shell}$ quantum-well nanoshell geometry. The energy offset at CdSe/CdS interfaces gives rise to strongly localized holes and quasi-localized electrons, which wave functions could extend over the entire nanocrystal volume. (c). The stripe pumping configuration used for measurements of the amplified stimulated emission (insert) in $CdS_{bulk}/CdSe/CdS_{shell}$ nanoshell QD assemblies.

2. Results and Discussion

In comparison with bulk materials,[21,37] quantum-confined semiconductors tend to exhibit significantly higher rates of non-radiative Auger recombination processes,[38-41] which compromise their overall optical gain in lasing applications. This phenomenon could be traced to several unique features of colloidal NCs. First, Coulomb interactions underlying Auger processes are strengthened in small-size nanoparticles as a result of the spatial and dielectric confinement, which causes the Auger decay constant to decrease proportionally to the volume occupied by photoinduced charges.[40] Another issue concerns a sharp potential gradient at core/shell interfaces, which leads to increased overlap between the initial and the final state involved in the Auger recombination process.[42] According to theoretical predictions,[42,43] alloyed interfaces with smoothed confinement potential in the heterostructure can drastically diminish Auger recombination rates by more than three orders of magnitude with respect to that of an abrupt interface. Finally, the conservation of translational momentum, which typically mitigates Auger recombination in bulk semiconductors,[44,72] is relaxed in zero-dimensional semiconductor NCs. In light of these limitations, the architecture of semiconductor nanocrystals for laser gain media has continuously evolved over the years. Zero-dimensional nanocrystals have been gradually replaced with morphologies that offered a larger confinement volume and a smoothed confinement potential. Among those, CdS/CdSe/CdS colloidal nanoplatelets and alloyed CdSe/CdS core/shell QDs have shown superior optical gain performance to date. A combination of a near unity PL quantum yield, large confinement volume, and smoothed potential at interfacial boundaries in these nanostructures has thus far enabled ASE threshold fluences in the 6-26 μJ/cm^2 range.[30,45]

Colloidal nanoshell QDs represents another nanoscale geometry, which could potentially result in the strong suppression of Auger recombination processes. The key advantage of the bulk-seeded "nanoshells" is associated with the ability to preserve the radial confinement of photoinduced charges regardless of the particle size. Consequently, all three dimensions of

nanoshell QDs could exceed the exciton Bohr radius enabling a significant increase in the exciton confinement volume (Fig. SF1), which leads to the reduction of Auger recombination rates. Thus far, the primary obstacle preventing the utilization of nanoshell QDs in light-emitting applications has been a somewhat low emission QY. Both inner and outer surfaces of the CdSe layer in CdS_{bulk}/CdSe/CdS_{shell} nanoshell QDs could exhibit strain-induced dislocations due to imperfectly grown interfaces. Furthermore, in contrast to strongly fluorescent, small-core CdS/CdSe/CdS_{shell} (d_{core} < 2.6 nm) spherical quantum wells[46-57] (QY > 90%), bulk-seeded nanoshell QDs have a particularly large total CdSe surface area, where defect states are more likely to yield exciton dissociation and carrier trapping.

The challenge of fabricating a highly-emissive CdSe quantum-well layer within a CdS_{bulk}/CdSe/CdS_{shell} nanoshell QD is largely synthetic in nature. It is related to the fact that the narrow-gap semiconductor of the shell domain (CdSe) is less reactive than that of the core (CdS).[58] This appears to be a general problem for chalcogenide-based core/shell NCs, where the electronegativity of oxygen group elements decreases with the atomic number, causing narrow gap semiconductors to exhibit a lower reactivity as compared to wider-gap materials of the same cation group. To address this issue, we have developed an alternative synthetic approach for core/shell nanostructures, which takes the advantage of particle aggregative growth in ligand-saturated solutions.[59,60] In a typical procedure, CdS bulk-size core nanoparticles were loaded in a flask containing a high concentration of oleylamine (> 60% by volume), along with Cd and Se ionic precursors (alternatively one can use small-diameter CdSe NCs in *lieu* of ionic precursors[58]). A gradual increase in the reaction temperature resulted in the formation of small-diameter CdSe NCs, which could be identified in the absorption spectra of the growth solution (**Fig. 2a**), as well as in TEM images of the reaction intermediate. Due to a high concentration of ligands in the growth solution, CdSe nuclei coalesced onto CdS_{bulk} seeds at temperatures near T_c = 220-230 C°. According to Fig. 2b, at this stage, any spectral features corresponding to isolated NCs have

disappeared, giving rise to a step-like CdSe absorption at λ = 590 nm. TEM images of the reaction product at this stage confirmed that most of the isolated CdSe NCs have attached to the surface of the CdS_{bulk} NCs. Notably, the homogenous coalescence of small CdSe clusters during the shell growth was likely to take place on par with the heterogeneous attachment of CdSe clusters to CdS surfaces. This could explain the presence of large size CdSe domains on the surface of the CdS_{bulk}/CdSe intermediate product (**Fig. 2b**). Finally, heating the reaction mixture to 240 C˚ for up to half an hour has allowed smoothing out the coalescence boundaries (Figs. 2c and 2d) and reduction of the particle size dispersion. Typically, maintaining the reaction temperature at 240 C˚ for about 10 min has resulted in the maximum CdS_{bulk}/CdSe emission QY of 3-4%, with the average particle size dispersion of 8.4% (Fig. SF2). Longer heating times, however, promoted excessive alloying of CdS_{bulk}/CdSe core/shell nanostructures, ultimately leading to the loss of band gap emission from the surface layer.

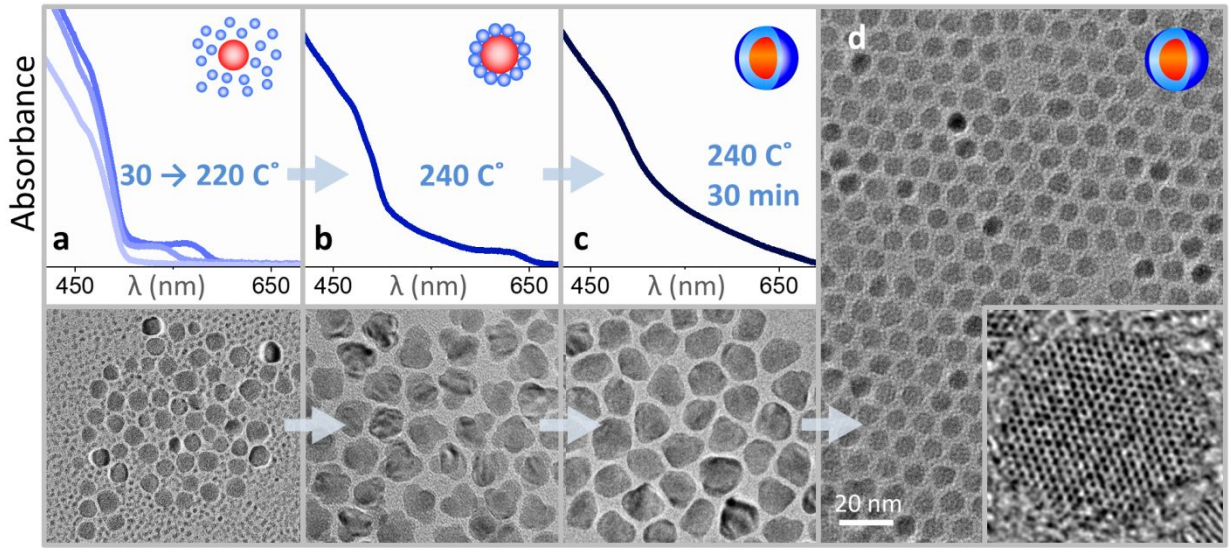

Figure 2. Coalescence-driven synthesis of CdS_{bulk}/CdSe nanoshell QDs. (a). The formation of isolated CdSe NCs is observed upon heating of the (Cd, Se precursor + CdS_{bulk}) reaction mixture from 30 to 220 ˚C. The TEM image confirms the formation of small CdSe NCs alongside CdS_{bulk} seeds. (b). Isolated CdSe NCs undergo a thermal coalescence on the surface of CdS_{bulk} when the temperature reaches 240 ˚C. (c). The subsequent ripening of core/shell nanoparticles results in alloying of CdS/CdSe interfaces and reshaping of nanoparticles into spheres. PL QY is maximized approximately 10-15 min of ripening at T = 240 ˚C (d). A characteristics TEM image of OLAM-capped CdS_{bulk}/CdSe nanoshells used for the synthesis of reported CdS_{bulk}/CdSe/CdS_{shell} quantum well QDs.

As-prepared CdS_{bulk}/CdSe NCs exhibited a rather modest PL intensity (**Fig. 3a**). The presence of a secondary emission feature at sub-band gap energies (λ = 700-900 nm) was ascribed to the emission from CdSe trap states that were presumably populated by the transfer of photoinduced charges to surface dangling bonds. This broad-band emission signal was quenched upon the deposition of a CdS surface-passivating shell giving rise to a single emission peak from the CdSe layer in CdS_{bulk}/CdSe/CdS_{shell} quantum-well QDs (Fig. 3b). The PL quantum yield of CdS_{bulk}/CdSe/CdS_{shell} nanoshell colloids has gradually improved with the increasing CdS shell thickness (ΔH_{CdS}) reaching its maximum for $\Delta H_{CdS} \approx 4$ nm. The PL QY of our best sample was estimated at 30%, nevertheless, other batches of CdS_{bulk}/CdSe/CdS_{shell} nanoshell QDs, grown from the same CdS_{bulk}/CdSe seeds, showed somewhat lower emission QYs, ranging between 10% and 17% (see Fig. SF2). We expect that with further synthetic improvements, it would be possible to achieve a more consistent CdS shell growth and a greater emission QY for the final product.

One of the key benefits of the digestive ripening growth approach lies in the ability to maintain a relatively narrow distribution of particle sizes. According to TEM images of as-prepared CdS_{bulk}/CdSe NCs (d_{CdS} = **7**.4-nm /ΔH_{CdSe} = 1.0 nm), nanoparticle shapes appeared nearly monodisperse with the corresponding standard size deviation of Δd = 8.4%, (see Figs. SF3b for the statistical analysis of particle sizes). Considering that the standard size deviation of original CdS_{bulk} "core" nanoparticles was only slightly lower (Δd = 8.1%, Fig. SF4), we expect the thickness of the CdSe light-emitting layer to be fairly uniform. A low dispersion of the CdSe shell thickness was also evident from a relatively narrow emission linewidth (Fig. 3b, red curve) in fully grown CdS_{bulk}/CdSe/CdS_{shell} nanoshell QDs (d_{CdS} = **7**.4-nm /ΔH_{CdSe} = 1.0 nm/ ΔH_{CdS} = 4.2-nm). The assigned thickness of the shell was determined by comparing the TEM diameters of CdS and

CdS/CdSe quantum dots. The total particle size dispersion for these nanostructures was estimated at 10% (Fig. SF2d).

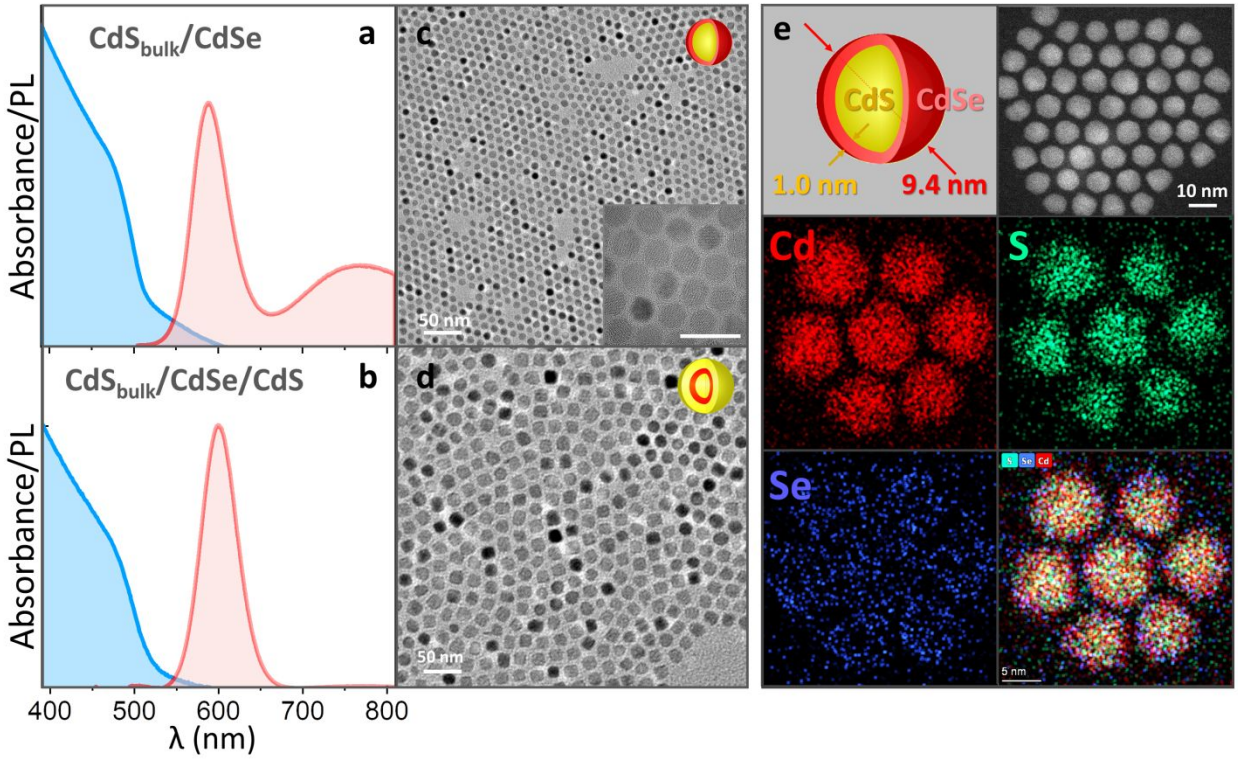

Figure 3. (a). Absorption and emission spectra of 9.4-nm CdS_{bulk}/CdSe nanoshell QDs comprising a 7.4-nm CdS core domain (see Fig. SF2 for the statistical size analysis). (b). Absorption and emission spectra of 17.9-nm CdS_{bulk}/CdSe/CdS_{shell} nanoshell QDs (d_{CdS} = **7**.4-nm /ΔH_{CdSe} = 1.0 nm/ ΔH_{CdS} = 4.2-nm). (c). A characteristic TEM image of CdS_{bulk}/CdSe nanoshell QDs (d_{CdS} = **7**.4-nm /ΔH_{CdSe} = 1.0 nm). The scale bar in the insert is 20 nm. (d). A characteristic TEM image of CdS_{bulk}/CdSe/CdS_{shell} nanoshell QDs. (e). High angle annular dark field (HAADF)-STEM imaging of 9.4-nm CdS_{bulk}/CdSe nanoshell QDs.

In order to investigate ASE, CdS_{bulk}/CdSe/CdS_{shell} nanoshell QDs were processed by drop-casting onto a glass substrate and were photoexcited using frequency-doubled pump pulses from an amplified Ti:sapphire laser system. The excitation beam was focused to a stripe by means of a cylindrical lens (see Fig. 1c) allowing for the collection lens to be placed perpendicular to the excitation direction. The onset of ASE was evident as a spectrally narrowed peak on the higher-energy side of the broader photoluminescence band (**Fig. 4**a), which appeared at pump fluences

exceeding a certain threshold. Further increases in the pump power caused the ASE feature to grow in intensity super-linearly (**Fig. 4a,b**). The blue shift of ASE relative to the band gap PL implies the repulsion of biexcitons,[61] which is consistent with the type II carrier delocalization across CdS/CdSe interfaces. The threshold for ASE was calculated by plotting the normalized integrated emission intensity versus the pump fluence (**Fig. 4b**). In case of the best-performing nanoshell sample, the threshold value was determined to be 38 μJ/cm^2. For comparison, the two other film samples developed using different-morphology nanoshell QDs resulted in ASE thresholds of 133 and 140 μJ/cm^2 (see Fig. SF5). The inferior optical quality of those films was most likely the reason for higher thresholds as any light scattering or haziness to films produces loss that is detrimental to the development of ASE. In the case of the best performing sample (38 μJ/cm^2), the amount of light scattering from the film was minimal.

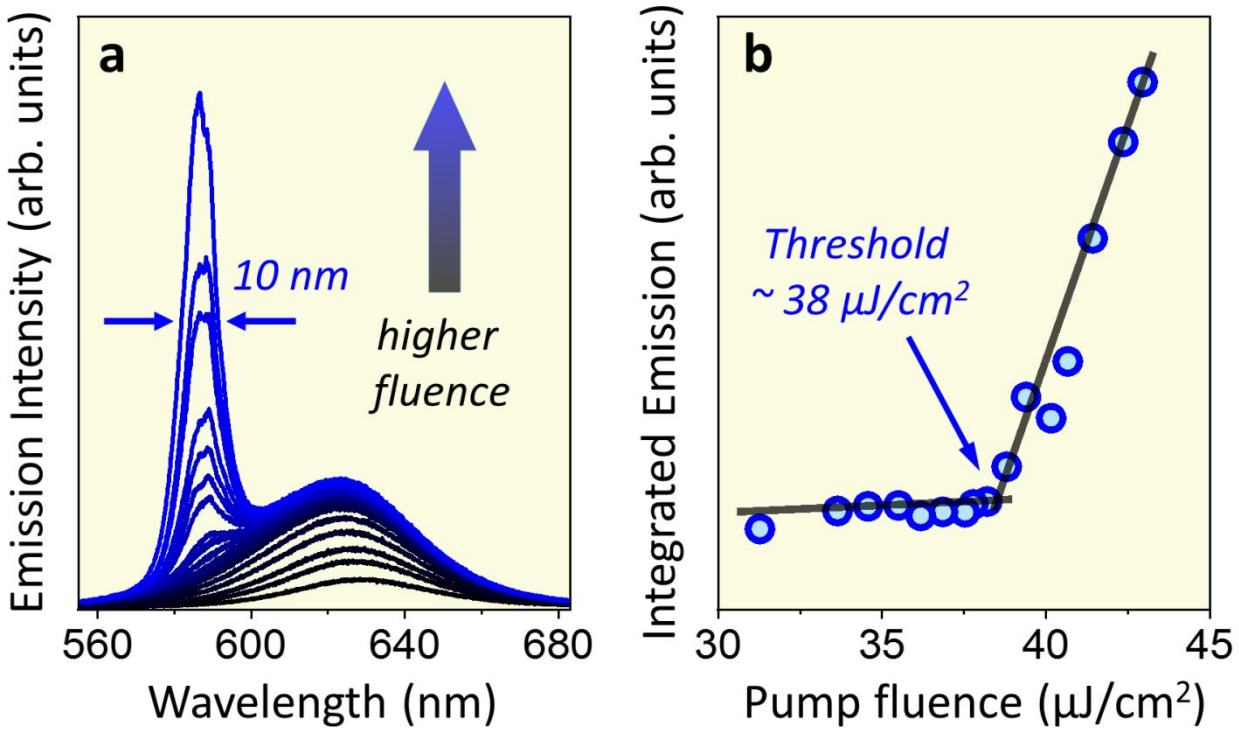

Figure 4. (a). Emission spectra observed from assemblies of 17.9-nm CdS_{bulk}/CdSe/CdS_{shell} (d_{CdS} = 7.4-nm /ΔH_{CdSe} = 1.0 nm/ ΔH_{CdS} = 4.2-nm) nanoshell QDs for different pump fluences. The narrow ASE peak with a FWHM of ~10 nm is observed with increasing excitation power. (b).

Normalized integrated emission intensity from films of $CdS_{bulk}/CdSe/CdS_{shell}$ QDs versus the pump fluence. The dots are experimental data, and the black lines are two linear fits for different regions of pump fluence.

The ASE threshold of nanoshell QD assemblies was at least an order of magnitude greater than previously reported for vacuum-deposited organic semiconductors[62] or epitaxial multiple-quantum-wells.[63] Nevertheless, the observed excitation fluence was comparable to ASE thresholds of other semiconductor NC morphologies. For instance, the lowest reported ASE threshold value for chalcogenide QDs was reported for CdS/CdSe/CdS nanoplatelets (6 $\mu J/cm^2$), which currently represents one of the best-performing QD gain media. The typical range of ASE thresholds (under femtosecond excitation) for such nanostructures is 6-53 $\mu J/cm^2$.[16,64] It should be noted, however, that the PL QY for nanoplatelets is considerably greater than that of nanoshell QDs (>90% vs 30%),[65] which could play an important role in lowering the threshold fluence. Beyond nanoplatelets, QD gain media was also developed using giant core/shell CdSe/CdS NCs,[24] exhibiting an ASE threshold of 26 $\mu J/cm^2$, CdSe/CdTe type II nanoplatelets, with ASE threshold of 43 $\mu J/cm^2$,[66] alloyed CdSe/CdS/ZnS core/shell NCs with best reported threshold of 44 $\mu J/cm^2$,[25,67,68] and finally, CdSe/CdS nanorods and tetrapods showing ASE threshold values in the 70-150 $\mu J/cm^2$ range.[27-29]

Considering the important role of Auger recombination dynamics on the performance of semiconductor NC gain media, we examined the characteristic timescales for both ASE and non-radiative (Auger) recombination processes in fabricated $CdS_{bulk}/CdSe/CdS_{shell}$ nanoshell QDs. To this end, we measured the ultrafast dynamics of multi-exciton populations by performing femtosecond transient absorption and time-resolved PL measurements.

The femtosecond pump-probe transient absorption spectroscopy was employed first to estimate the biexciton lifetime of nanoshell QD samples in solution. Details of the optical setup and sample preparation are described in the experimental section. In brief, we have chosen two excitation regimes corresponding to pump photon energies lying above (λ = 420 nm) and below

(λ = 510 nm) the CdS band gap **(Fig. 5)**. Under these conditions, higher-energy pump photons could induce the exciton population both in CdS and CdSe domains of nanoshells, while the lower-energy excitation regime was expected to populate excited states predominantly in the CdSe layer. For both excitations modes, the recovery of excited-state populations was probed in the λ = 400-650 nm spectral window, where CdS and CdSe band gap transitions could be simultaneously observed. The pump power was adjusted using neutral density filters to produce an average exciton population of <N> ≈ 1 per single nanocrystal (after taking into account the photoinduced charge transfer contribution in Fig. 5c).

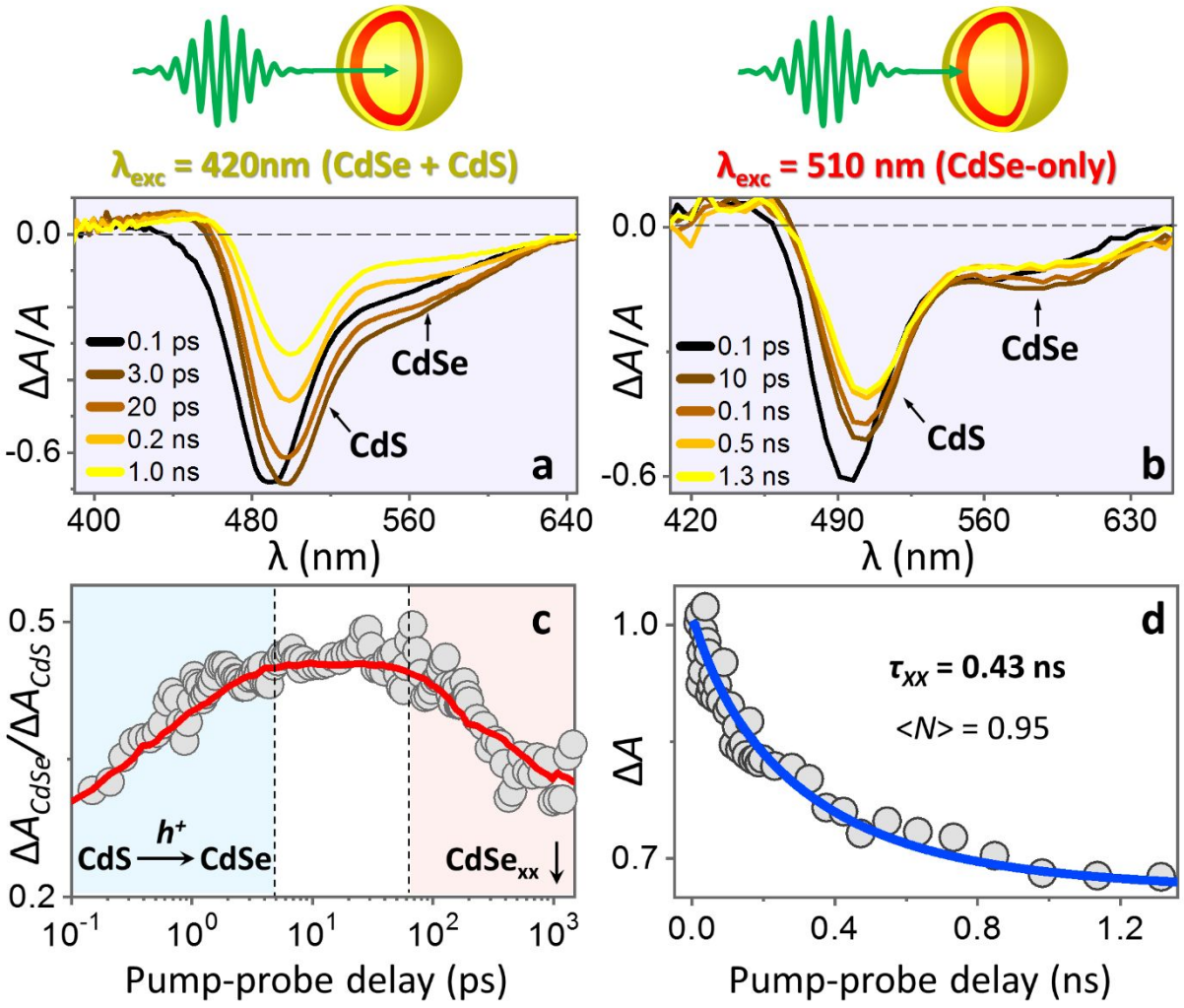

Figure 5. Time-resolved transient absorption measurements of $CdS_{bulk}/CdSe/CdS_{shell}$ nanoshell QDs. (a). TA bleach recovery of 17.9-nm $CdS_{bulk}/CdSe/CdS_{shell}$ nanoshell QDs excited above the

CdS band edge (λ = 420 nm). The two bleach regions centered at λ = 495 nm and λ = 575 nm, correspond to populations of the lowest-energy band gap transitions in CdS_{bulk} and CdSe domains, respectively. (b). The TA bleach recovery of 17.9-nm CdS_{bulk}/CdSe/CdS_{shell} nanoshell QDs excited at λ = 510 nm. The lowest-energy band gap transitions in CdS_{bulk} and CdSe domains were observed at λ = 490 nm and λ = 585 nm, respectively. (c). The ratio of the CdSe bleach amplitude (ΔA_{CdSe}) to that of CdS (ΔA_{CdS}) versus the pump-probe delay. The early rise of this ratio (τ < 4 ps) is attributed to the CdS → CdSe charge transfer. The subsequent decline of this ratio at τ > 100 ps suggests a faster relaxation of CdSe excitations, presumably due to the biexciton contribution. (d). The temporal evolution of the TA bleach in 17.9-nm CdS_{bulk}/CdSe/CdS_{shell} nanoshell QDs excited at λ = 510 nm (grey circles). The experimental data was fitted using model calculations based on statistical scaling of Auger lifetimes and Poisson distribution of initial multi-exciton populations. The biexciton lifetime was estimated to be τ_{xx} = 0.43 ns.

Figure 5a shows chirp-corrected TA spectra of 17.9-nm CdS_{bulk}/CdSe/CdS_{shell} nanoshell QDs, excited at λ = 420 nm. Out of the two spectral regions showing negative ΔA, the stronger signal (λ ≈ 495 nm) was attributed to the excitation-induced state filling of band-gap transitions in the CdS domain, while the second TA bleach, observed at lower energies (λ = 560 – 640 nm), was attributed to the lowest-energy transition in the CdSe shell. The ratio of these signals, $\Delta A_{CdSe}/\Delta A_{CdS}$ (Fig. 5c), showed a two-fold increase at early pump-probe times (τ < 4 ps), consistent with a photoinduced charge transfer between CdS and CdSe domains. Due to a high degeneracy of hole levels in chalcogenide NCs, the TA bleach of band edge transitions in both CdS and CdSe domains was attributed to the occupation of electron states in the conduction band. Under this assumption, the early rise of the $\Delta A_{CdSe}/\Delta A_{CdS}$ ratio was ascribed to the delocalization of CdS electrons into the CdSe shell. At longer pump-probe delays (τ = 100 - 1000 ps), the $\Delta A_{CdSe}/\Delta A_{CdS}$ ratio was observed to decline, signaling a faster loss of excitations in the CdSe shell relative to that of CdS. Considering that multi-exciton populations in CdSe are subject to Auger decay, such a drop in the $\Delta A_{CdSe}/\Delta A_{CdS}$ ratio could indicate the process of biexciton loss, with an approximate time scale of several hundreds of picoseconds.

To perform a more accurate determination of biexciton lifetimes in 17.9-nm $CdS_{bulk}/CdSe/CdS_{shell}$ nanoshell QDs, we used a lower-photon-energy excitation regime ($\lambda \approx 510$ nm). Under these conditions, pump photons were predominantly captured by the CdSe domain of nanoshells, since band gap transitions of the CdS component were mostly higher in energy ($\lambda_{gap} \approx$ 490 nm, see Fig. SF4a). Interestingly, the CdS bleach corresponding to the higher-energy side of the pump spectral range was observed almost immediately after the excitation, indicating a possible absorption of photons into delocalized CdS(e) – CdSe(h) states. Similar behavior has been observed for CdSe-CdS dot-in-a-rod systems via TA and THz spectroscopy measurements.[69-71] The amplitude of this ΔA band exceeded that of the CdSe TA bleach, centered around $\lambda \approx 585$ nm. To determine the average lifetime of biexcitons, the recovery kinetics for the ΔA_{CdSe} bleach (Fig. 5d) was fitted by using model calculations based on the coupled rate equation formalism[1] (see the SI section). Briefly, the ΔA_{CdSe} signal was assumed to be contributed by up to four excitons, such that the average number of excitons per nanocrystal was expressed as: $P(t) = 4 \times P(4,t) + 3 \times P(3,t) + 2 \times P(2,t) + P(1,t)$. The lifetime for each multi-exciton state, τ_n, was computed using a statistical scaling law: $\tau_n^{-1} = n^2(n-1)\tau_2^{-1}/4$,[21] while the single exciton lifetime of τ_1(CdSe) = 101 ns was derived from the PL intensity decay data (Fig. SF6). The resulting model parametric curve, $P(\tau_{xx}, t)$, was then fitted to the experimental TA kinetics for the CdSe bleach, ΔA(t), in order to determine the best fitting parameter, τ_{xx}.

The best fit of the experimental data with the multi-exciton population curve, $P(t)$, has yielded the average biexciton lifetime of $\tau_{xx} = 430$ ps (see Fig. 5d). This value was somewhat lower than biexciton lifetimes of larger-core nanoshell samples (τ_{xx} = 0.5-1.2 ns) reported previously in Ref. 36. The decrease in τ_{xx} of present samples was consistent with a reduced volume of the CdSe

light-emitting layer for nanoshells fabricated in this work, as the rate of Auger processes is expected to diminish linearly with the nanoparticle volume ($\Gamma^{-1} \sim V^{0.9\text{-}1.1}$).[38,39,42,72,73]

The ASE dynamics was inferred from the photoluminescence decay of nanoshell QD films. In order to observe the competition between Auger and ASE processes, the samples were excited at pump fluences both below and above ASE thresholds, as shown in **Fig. 6**. Above the ASE threshold, the photoluminescence spectral profile exhibited a narrow feature associated with the stimulated emission (Fig. 6, insert). At low pump fluencies (red and blue curves), this feature was absent and the PL decay was dominated by Auger recombination. We speculate that at the lowest pump fluence (4μJ/cm^2, blue curve), the PL decay was dominated by single excitons, which could also include some trapping that produced a faster decay. For instance, the analysis of the "8 μJ/cm^2" – "4 μJ/cm^2" PL spectral difference (Fig. SF7c) results in a differential signal, which can be fitted to a lifetime of 220 ± 8 ps. At a higher pump fluence of 25 μJ/cm^2, the PL spectral difference ("25 μJ/cm^2" – "4 μJ/cm^2") appears to decay faster (τ = 121 ps, Fig. SF7b), suggesting that more than 2 excitons are excited on average at this intensity. Above the lasing threshold (46 μJ/cm^2, black curve), the characteristic time scale for the stimulated emission appears to be an order of magnitude shorter than the Auger recombination time, determined independently from TA measurements (τ_{xx} = 430 ps). Consequently, Auger recombination offered little competition to ASE, leading to low thresholds.

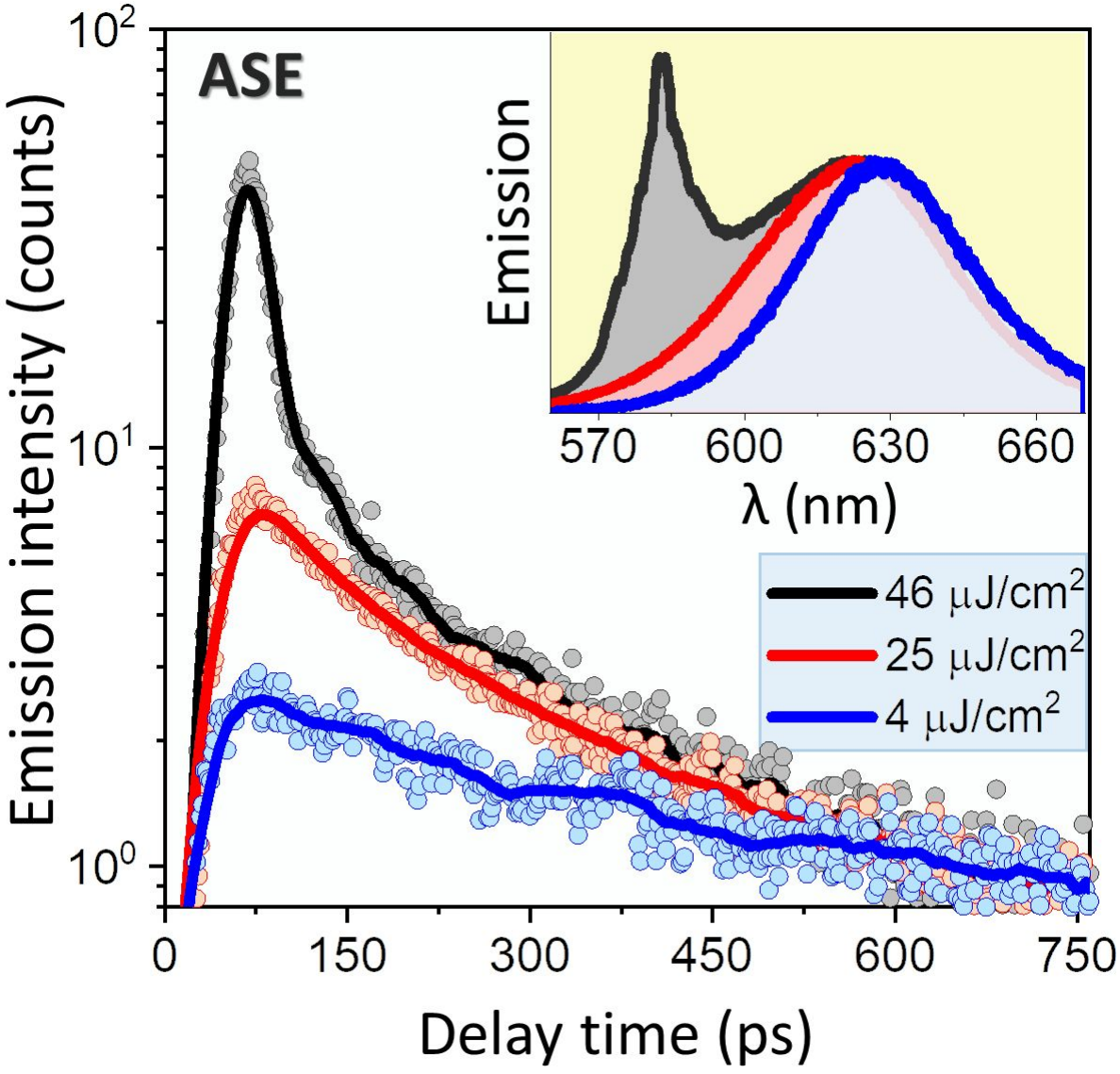

Figure 6. Time-resolved transient PL intensity for $CdS_{bulk}/CdSe/CdS_{shell}$ QDs measured at the peak emission wavelength for three excitation levels. The insets show the corresponding emission spectra, indicating the ASE threshold below 46 μJ/cm^2.

3. Conclusion

In conclusion, we have demonstrated that $CdS_{bulk}/CdSe/CdS_{shell}$ nanoshell QDs represent a promising class of colloidal QDs for the development of laser active media. A combination of a large quantum-confinement volume and alloyed interfaces in these nanomaterials facilitates an efficient suppression of non-radiative Auger processes that typically compromise the optical gain

in QD lasers. Our best samples showed the onset of ASE at a low threshold fluence of 38 μJ/cm^2. We expect that with further improvements in nanoshell QD emission quantum yield, presently estimated at 30%, the ASE threshold could be further reduced, allowing these materials to become a competitive QD morphology for the development of optical gain media.

4. Experimental section

Materials: The following materials were used: cadmium oxide (CdO, 99.5%, Aldrich), 1-octadecene (ODE, 90%, Aldrich), octadecylamine (ODA, 90%, Acros), oleic acid (OA, 90%, Aldrich), sulfur (S, 99.999%, Acros), ethanol (anhydrous, BeanTown Chemical), chloroform (anhydrous, 99%, BeanTown Chemical), oleylamine (OLAM, tech., 70%, Aldrich), tri-n-octylphosphine (TOP, 90%, Acros), toluene (anhydrous, Aldrich, 99.8 %), octane (98 %, Aldrich), hexanes (Fisher, Certified ACS) mercaptopropyltrimethoxysilane (MPTA, 95 %, Aldrich)selenium powder (Se, 200 mesh, Acros), and acetone (anhydrous, Amresco, ACS grade). All reactions were performed under an argon atmosphere using the standard Schlenk line. The centrifuge (VWR Clinical 100) used for precipitation was operated at 6500 rpm.

Synthesis of bulk-size CdS nanocrystals: Bulk-size CdS nanocrystals ($d \approx 8$ nm) were synthesized using a previously reported digestive ripening technique.**Error! Bookmark not defined.** To this end, small-diameter CdS NC seeds ($d \approx 3$-4 nm) were loaded into 60:40 OLAM/ODE mixture (total volume of 7 mL) and degassed at 120 °C for 1 hour. The solution was subsequently heated up to 260 °C to promote interparticle coalescence. Once the desired nanoparticle size was reached (usually indicated by the loss of quantum confinement absorption features), the reaction was quenched by removing the flask from the heating mantle. The crude NC product was subsequently separated from the solution by precipitating with the addition of 4:1 acetone/ethanol mixture and subsequently redispersed in chloroform.

Synthesis of CdS_{bulk}/CdSe core/shell NCs: The deposition of the CdSe shell onto bulk-like CdS nanoparticles was performed through a slow injection of pre-mixed Cd and Se ionic precursors. The cadmium oleate precursor was prepared by first degassing of the mixture containing 0.034 g of CdO, 0.8 mL of OA, and 5 mL of ODE under vacuum at 120 °C for 2 hours. The flask was

switched to argon and heated up to 260 °C in order to obtain nearly colorless $Cd(oleate)_2$ solution, which was subsequently cooled down to room temperature. In a separate flask, 0.027 g of Se was dissolved in 1.8 mL of pre-pumped TOP at 120 °C until solution turned clear and then added to $Cd(oleate)_2$ at room temperature to form a mixture of Cd and Se precursors. To grow a CdSe shell, CdS_{bulk} NCs in chloroform were loaded into a mixture of 4 mL of OLAM and 10 mL of ODE followed by degassing at 120 °C. The reaction mixture was then switched to argon and heated up to 260 °C. The Cd/Se precursor was slowly injected into the reaction flask via a syringe pump at a rate of 3 mL/h. Once the desired CdSe shell size was reached, the reaction was stopped by removing the flask from the heating mantle. The product was separated from the solution by a single precipitation with the addition of a 4:1 acetone/ethanol mixture and re-dispersion in chloroform.

Synthesis of CdS_{bulk}/CdSe/CdS_{shell} nanoshell QDs: CdS surface-passivating layer was deposited using the SILAR method, according to Ref. 74. To this end, cadmium oleate precursor was prepared similarly to the previous step. In the second flask, 0.013 g of S was added to 1.8 mL of ODE and heated up to 200 °C and kept for 5-7 minutes until solution turns dark yellow color. Both solutions were combined together at room temperature under an argon flow. For CdS shell deposition, a mixture of CdS_{bulk}/CdSe seeds in chloroform, 1.5g of ODA, and 6.33 mL of ODE was transferred to the reaction flask and degassed at 70 °C for 1 h. Subsequently, the mixture was switched to Ar, heated up to 240 °C. As long as no changes in the CdS/CdSe PL were observed, the precursor mixture was injected into the flask using a syringe pump at a rate of 1 mL/h. Once the desired shell size was reached, the reaction was stopped by removing the flask from the heating mantle. Finally, the product was separated from the solution by precipitation with the addition of a 4:1 acetone/ethanol mixture and stored in chloroform.

Characterization: Ultraviolet−visible absorption spectra were recorded using a CARY 60 scan spectrophotometer. High-resolution transmission electron microscopy (TEM) measurements were carried out using a JEOL JEM-3011UHR instrument operated at 300 kV. Specimens were prepared by depositing a diluted drop of NCs solution in organic solvent onto a carbon-coated copper grid and allowing it to dry in air. Luminescence spectra were recorded using a 400 nm PicoQuant PDL 800-D pulsed laser and measured with an Andor Newton detector. Time-resolved emission lifetime spectra were recorded using the same 400-nm pulsed laser, and photons were collected and

processed using a SPC-130 TCSPC module from Boston Electronics. Relative quantum yield measurements were acquired using a GS32 Intelite 532 nm CW DPSS laser (a Cyanine3 NHS ester dye obtained from Lumiprobe was used as the reference).

Transient Absorption Measurements: The femtosecond transient absorption measurements were performed using a regeneratively amplified Ti:sapphire laser system (Hurricane, Spectra-Physics) that generates a 1 kHz train of 90 fs (fhwm), 0.9 mJ pulses centered at 800 nm. The amplified beam is split at a 50:50 ratio. The first component is sent to a TOPAS-C optical parametric amplifier to produce the 420 nm (or 510 nm) pulses used for sample excitation. The second beam is attenuated, sent through a computer-controlled optical delay stage, and then focused onto a 3 mm CaF_2 window to produce a white-light continuum (wlc) probe spanning the range of 345−760 nm. The wlc probe beam was focused to a 75 μm diameter spot at the sample position and overlapped at a 6° angle with the excitation beam focused to a 150 μm-diameter spot. A fraction of the wlc probe beam was split off before the sample to be utilized as a reference for the correction of shot-to-shot pulse intensity fluctuations. The probe (after the sample) and reference beams were dispersed by a spectrograph and recorded using a dual 512-pixel diode array detector synchronized to the 1 kHz repetition rate. The difference between the decadic logarithms of a probe-to-reference pulse intensity ratio was measured at a specific position of the optical stage for the case in which the excitation pulse was on and off. Typically, 300 on and off pairs were averaged to produce the transient absorption signal (ΔA) at the corresponding delay time, and then the procedure was repeated for ~20 scans of the optical delay stage. The solutions were kept in a 1 mm path length cell or in a spinning 2 mm path length cuvette. These two sets of conditions did not have any noticeable difference in terms of the time and spectral evolution of transient absorption signals. The zero delay time positions at different probe wavelengths were obtained from nonresonant electronic responses from a neat $CHCl_3$ solvent measured under the same experimental conditions and used for the chirp correction of the measured ΔA data. The typical excitation energy was 0.5 μJ/pulse. The linearity of ΔA signals with excitation energy confirmed that single-photon excitation is responsible for the measured data. The polarization of the excitation beam was set at the magic angle (54.7°) with respect to the probe beam to eliminate signals from rotational dynamics of the solute. All experiments were performed at 21 °C.

Amplified Stimulated Emission Measurements and Dynamics: Thin-film samples of nanocrystals were prepared for measurements by first performing an additional anti-solvent precipitation with ethanol, then redispersing the samples in 9:1 hexane: octane. The concentrated solutions were drop-cast on to microscope slides treated with MPTS (24 hours as 5 MPTS w/v % in dry toluene). This sample displaying the lowest threshold ASE was an opalescent, non-scattering film; other samples showed perceptible haze. To excite samples, a 2 kHz, 35 fs amplified Ti: sapphire laser (Spectraphysics) was frequency doubled to 400 nm and the beam was focused on the sample as a stripe with a cylindrical lens, with the edges of the stripe defined by razor blades. Emission was collected via a lens positioned normal to the excitation beam and fiber-coupled to a CCD through a monochromater (Princeton), for spectral data acquisition, or to a streak camera (Hamamatsu) for time-resolved data collection.

Supporting information.

Experimental section, additional figures and details of calculation.

Acknowledgment.
This work was supported by the Award DE-SC0016872 (MZ) funded by the U.S. Department of Energy, Office of Science. JC was supported in part by NSF Award DMR-1710063. The authors acknowledge the financial support of the University of Michigan College of Engineering and NSF grant #DMR-9871177, and technical support from the Michigan Center for Materials Characterization. This work was performed, in part, at the Center for Nanoscale Materials, a U.S. Department of Energy Office of Science User Facility, and supported by the U.S. Department of Energy, Office of Science, under Contract No. DE-AC02-06CH11357. A.N.T acknowledges NSF awards CHE-0923360 and CHE-1626420.

References

[1] V. I. Klimov, A. A. Mikhailovsky, S. Xu, A. Malko, J. A. Hollingsworth, C. A. Leatherdale, H.-J. Eisler, M. G. Bawendi, *Optical Gain and Stimulated Emission in Nanocrystal Quantum Dots Science.* 2000*,* **290**, 314–317.

[2] D. V. Talapin, J.-S. Lee, M. V. Kovalenko, E. V. Shevchenko, *Prospects of Colloidal Nanocrystals for Electronic and Optoelectronic Applications. Chem. Rev.* 2010, **110**, 389-458.

[3] M. V. Kovalenko, L. Manna, A. Cabot, Z. Hens, D. V. Talapin, C. R. Kagan, V. I. Klimov, A. L. Rogach, P. Reiss, D. J. Milliron, P. Guyot-Sionnest, G. Konstantatos, W. J. Parak, T. Hyeon, B. A. Korgel, C. B. Murray, W. Heiss, *Prospects of Nanoscience with Nanocrystals. ACS Nano.* 2015, **9**, 1012-1057.

[4] Y. Arakawa, H. Sakaki, *Multidimensional quantum well laser and temperature dependence of its threshold current*. *Appl. Phys. Lett.* 1982, **40**, 939–941.

[5] S. Chen, W. Li, J. Wu, Q. Jiang, M. Tang, S. Shutts, S. N. Elliott, A. Sobiesierski, A. J. Seeds, I. Ross, P. M. Smowton, H. Liu, *Electrically pumped continuous-wave III–V quantum dot lasers on silicon. Nat. Photon.* 2016, **10**, 307-311.

[6] H. Liu, T. Wang, Q. Jiang, R. Hogg, F. Tutu, F. Pozzi, A. Seeds, *A. Long-wavelength InAs/GaAs quantum-dot laser diode monolithically grown on Ge substrate. Nat. Photon.* 2011, **5**, 416-419.

[7] M. Asada, Y. Miyamoto, Y. Suematsu, *Gain and the threshold of three-dimensional quantum-box lasers*. *IEEE J. Quant. Electron.* 1986, **22**, 1915–1921.

[8] Y. Wang, H. Sun, *Advances and prospects of lasers developed from colloidal semiconductor nanostructures. Prog. Quant. Electron.* 2018, **60**, 1-29.

[9] Y. Chen, J. Herrnsdorf, B. Guilhabert, Y. Zhang, I. M. Watson, E. Gu, N. Laurand, M. D. Dawson, *Colloidal quantum dot random laser. Opt. Express.* 2011, **19**, 2996–3003.

[10] C. B. Murray, D. J. Norris, M. G. Bawendi, *Synthesis and characterization of nearly monodisperse CdE (E = sulfur, selenium, tellurium) semiconductor nanocrystallites. J. Am. Chem. Soc.* 1993, **115**, 8706-8715.

[11] A. P. Alivisatos, *Semiconductor Clusters, Nanocrystals, and Quantum Dots. Science.* 1996*,* **271**, 933–937.

[12] J. S. Steckel, P. T. Snee, S. Coe-Sullivan, J. P. Zimmer, J. P. Halpert, P. Anikeeva, L. Kim, V. Bulovic, M. G. Bawendi, *Color-Saturated Green-Emitting QD-LEDs. Angew. Chemie.* 2006**,** **45**, 5796–5799.

[13] Y. Zhu, W. Xie, S. Bisschop, T. Aubert, E. Brainis, P. Geiregat, Z. Hens, *On-Chip Single-Mode Distributed Feedback Colloidal Quantum Dot Laser under Nanosecond Pumping*. *ACS Photonics.* 2017*,* **4**, 2446–2452.

[14] S. Yakunin, L. Protesescu, F. Krieg, M. I. Bodnarchuk, G. Nedelcu, M. Humer, G. De Luca, M. Fiebig, W. Heiss, M. V. Kovalenko, *Low-threshold amplified spontaneous emission and lasing from colloidal nanocrystals of caesium lead halide perovskites. Nat. Commun.* 2015*,* **6**, 8056.

[15] Y. Wang, X. Li, J. Song, L. Xiao, H. Zeng, *All-Inorganic Colloidal Perovskite Quantum Dots: A New Class of Lasing Materials with Favorable Characteristics. Adv. Mater.* 2015*,* **27**, 7101–7108.

[16] J. Q. Grim, S. Christodoulou, F. Di Stasio, R. Krahne, R. Cingolani, L. Manna, I. Moreels, *Continuous-wave biexciton lasing at room temperature using solution-processed quantum wells. Nat. Nanotechnol.* 2014*,* **9**, 891-895.

[17] Z. Yang, M. Pelton, I. Fedin, D. V. Talapin, E. Waks, *A room temperature continuous-wave nanolaser using colloidal quantum wells. Nat. Commun.* 2017*,* **8**, 143.

[18] P. Chhantyal, S. Naskar, T. Birr, T. Fischer, F. Lübkemann, B. N. Chichkov, D. Dorfs, N. C. Bigall, C. Reinhardt, *Low Threshold Room Temperature Amplified Spontaneous Emission in 0D, 1D and 2D Quantum Confined Systems. Sci. Rep.* 2018*,* **8**, 3962.

[19] M. Pelton, *Carrier Dynamics, Optical Gain, and Lasing with Colloidal Quantum Wells. J. Phys. Chem. C.* 2018*,* **122**, 10659−10674.

[20] F. Todescato, I. Fortunati, A. Minotto, R. Signorini, J. J. Jasieniak, R. Bozio, *Engineering of Semiconductor Nanocrystals for Light Emitting Applications. Materials.* 2016*,* **9**, 672.

[21] V. I. Klimov, A. A. Mikhailovsky, D. W. McBranch, C. A. Leatherdale, M. G. Bawendi, *Quantization of Multiparticle Auger Rates in Semiconductor Quantum Dots. Science.* 2000*,* **287**, 1011–1013.

[22] V. A. Kharchenko, M. Rosen, *Auger relaxation processes in semiconductor nanocrystals and quantum wells. J. Lumin.* 1996*,* **70**, 158–169.

[23] Y. Chan, J.-M. Caruge, P. T. Snee, M. G. Bawendi, *Multiexcitonic two-state lasing in a CdSe nanocrystal laser. Appl. Phys. Lett.* 2004*,* **85**, 2460.

[24] F. Garcia-Santamaria, Y. Chen, J. Vela, R. D. Schaller, J. A. Hollingsworth, V. I. Klimov, *Suppressed Auger Recombination in "Giant" Nanocrystals Boosts Optical Gain Performance. Nano Lett.* 2009*,* **9**, 3482−3488.

[25] C. H. Lin, E. Lafalce, J. Jung, M. J. Smith, S. T. Malak, S. Aryal, Y. J. Yoon, Y. Zhai, Z. Lin, Z. V. Vardeny, V. V. Tsukruk, *Core/Alloyed-Shell Quantum Dot Robust Solid Films with High Optical Gains. ACS Photonics.*2016*,* **3**, 647−658.

[26] M. Zavelani-Rossi, M. G. Lupo, R. Krahne, L. Manna, G. Lanzani, *Lasing in self-assembled microcavities of CdSe/CdS core/shell colloidal quantum rods. Nanoscale.* 2010*,* **2**, 931−935.

[27] H. Htoon, J. A. Hollingsworth, R. Dickerson, V. I. Klimov, *Effect of Zero- to One-Dimensional Transformation on Multiparticle Auger Recombination in Semiconductor Quantum Rods. Phys. Rev. Lett.* 2003*,* **91**, 227401.

[28] I. Moreels, G. Rainò, R. Gomes, Z. Hens, T. Stöferrle, R. F. Mahrt, *Nearly Temperature-Independent Threshold for Amplified Spontaneous Emission in Colloidal CdSe/CdS Quantum Dot-in-Rods. Adv. Mater.* 2012*,* **24**, OP231–OP235.

[29] Y. Liao, G. Xing, N. Mishra, T. C. Sum, Y. Chan, *Low Threshold, Amplified Spontaneous Emission from Core-Seeded Semiconductor Nanotetrapods Incorporated into a Sol–Gel Matrix Adv. Mater*. 2012*,* **24**, OP159−OP164.

[30] C. She, I. Fedin, D. S. Dolzhnikov, A. Demortière, R. D. Schaller, M. Pelton, D. V. Talapin, Low-*Threshold Stimulated Emission Using Colloidal Quantum Wells. Nano Lett.* 2014*,* **14**, 2772−2777.

[31] Y. Kelestemur, Y. Shynkarenko, M. Anni, S. Yakunin, M. L. De Giorgi, M. V. Kovalenko, *Colloidal CdSe Quantum Wells with Graded Shell Composition for Low-Threshold Amplified Spontaneous Emission and Highly Efficient Electroluminescence. ACS Nano.* 2019*,* **13**, 13899-13909.

[32] B. Guzelturk, M. Pelton, M. Olutas, H. V. Demir, *Giant Modal Gain Coefficients in Colloidal II−VI Nanoplatelets.* Nano Lett. 2019*,* **19**, 277−282.

[33] B. K. Chen, S. Chang, D. Y. Li, L. L. Chen, Y. T. Wang, T. Chen, B. S. Zou, H. Z. Zhong, A. L. Rogach. *Template Synthesis of $CuInS_2$ Nanocrystals from In_2S_3 Nanoplates and Their Application as Counter Electrodes in Dye-Sensitized Solar Cells. Chem. Mater.* 2015, **27**, 5949-595ot6.

[34] N. Razgoniaeva, P. Moroz, M. Yang, D. S. Budkina, H. Eckard, M. Augspurger, D. Khon, A. N. Tarnovsky, M. Zamkov, *One-Dimensional Carrier Confinement in "Giant" CdS/CdSe Excitonic Nanoshells. J. Am. Chem. Soc.* 2017*,* **139**, 7815-7822.

[35] N. Razgoniaeva, M. Yang, C. Colegrove, N. Kholmicheva, P. Moroz, H. Eckard, A. Vore, M. Zamkov, *Double-Well Colloidal Nanocrystals Featuring Two-Color Photoluminescence*. *Chem. Mater.* 2017*,* **29**, 7852-7858.

[36] N. Kholmicheva, D. S. Budkina, J. Cassidy, D. Porotnikov, D. Harankahage, A. Boddy, M. Galindo, D. Khon, A. N. Tarnovsky, M. Zamkov, *Sustained Biexciton Populations in Nanoshell Quantum Dots. ACS Photonics.* 2019*,* **6**, 1041-1050.

[37] D. I. Chepic, A. L. Efros, A. I. Ekimov, M. G. Ivanov, V. A. Kharchenko, I. A. Kudriavtsev, T. V. Yazeva, *Auger ionization of semiconductor quantum drops in a glass matrix. J. Lumin.* 1990, **47**, 113–127.

[38] I. Robel, R. Gresback, U. Kortshagen, R. D. Schaller, V. I. Klimov, *Universal Size-Dependent Trend in Auger Recombination in Direct-Gap and Indirect-Gap Semiconductor Nanocrystals*. *Phys. Rev. Lett.* 2009, **102**, 177404.

[39] V. I. Klimov, *Multicarrier Interactions in Semiconductor Nanocrystals in Relation to the Phenomena of Auger Recombination and Carrier Multiplication. Annu. Rev. Condens. Matter Phys.* 2014, **5**, 285-316.

[40] J. P. Philbin, E. Rabani, *Electron-Hole Correlations Govern Auger Recombination in Nanostructures. Nano Lett.* 2018, **18**, 7889-7895.

[41] P. Kambhampati, *Multiexcitons in Semiconductor Nanocrystals: A Platform for Optoelectronics at High Carrier Concentration*. *J. Phys. Chem. Lett.* 2012, **3**, 1182– 1190.

[42] G. E. Cragg, A. L. Efros, *Suppression of Auger Processes in Confined Structures*. *Nano Lett.* 2010, **10**, 313–317.

[43] J. I. Climente, J. L. Movilla, J. Planelles, *Auger Recombination Suppression in Nanocrystals with Asymmetric Electron–Hole Confinement. Small.*2012, **8**, 754–759.

[44] L. T. Kunneman, M. D. Tessier, H. Heuclin, B. Dubertret, Y. V. Aulin, F. C. Grozema, J. M. Schins, L. D. A. Siebbeles, *Bimolecular Auger Recombination of Electron–Hole Pairs in Two-Dimensional CdSe and CdSe/CdZnS Core/Shell Nanoplatelets. J. Phys. Chem. Lett.* 2013, **4**, 3574–3578.

[45] F. Fan, O. Voznyy, R. P. Sabatini, K. T. Bicanic, M. M. Adachi, J. R. McBride, K. R. Reid, Y.-S. Park, X. Li, A. Jain, R. Quintero-Bermudez, M. Saravanapavanantham, M. Liu, M. Korkusinski,

P. Hawrylak, V. I. Klimov, S. J. Rosenthal, S. Hoogland, E. H. Sargent, *Continuous-wave lasing in colloidal quantum dot solids enabled by facet-selective epitaxy. Nature.*2017*,* **544**, 75-79.

[46] E. P. Pokatilov, V. A. Fonoberov, V. M. Fomin, J. T. Devreese, *Electron and hole states in quantum dot quantum wells within a spherical eight-band model*. *Phys. Rev. B* 2001*,* **64**, 245329.

[47] E. A. Dias, J. I. Saari, P. Tyagi, P. Kambhampati, *Improving Optical Gain Performance in Semiconductor Quantum Dots via Coupled Quantum Shells. J. Phys. Chem. C* 2012*,* **116**, 5407-5413.

[48] P. Kambhampati, T. Mack, L. Jethi, *Understanding and Exploiting the Interface of Semiconductor Nanocrystals for Light Emissive Applications. ACS Photonics* 2017*,* **4**, 412-423.

[49] M. Braun, S. Link, C. Burda, M. El-Sayed, *Transfer times of electrons and holes across the interface in CdS/HgS/CdS quantum dot quantum well nanoparticles. Chem. Phys. Lett.* 2002*,* **361**, 446-452.

[50] J. Xu, M. Xiao, *Lasing action in colloidal CdS/ CdSe/ CdS quantum wells. Appl. Phys. Lett.* 2005, **87**, 173117.

[51] J. Xu, M. Xiao, D. Battaglia, X. Peng, *Exciton radiative recombination in spherical CdS/ CdSe/CdS quantum-well nanostructures. Appl. Phys. Lett.* 2005, **87**, 043107.

[52] D. Battaglia, J. J. Li, Y. Wang, X. Peng, *Colloidal Two-Dimensional Systems: CdSe Quantum Shells and Wells. Angew. Chem. Int. Ed.* 2003, **42***,* 5035-5039.

[53] J. Schrier, L.-W. Wang, *Electronic structure of nanocrystal quantum-dot quantum wells*. *Phys. Rev. B*. 2006, **73**, 245332.

[54] A. W. Schill, C. S. Gaddis, W. Qian, M. A. El-Sayed, Y. Cai, V. T. Milam, K. Sandhage, *Ultrafast Electronic Relaxation and Charge-Carrier Localization in CdS/CdSe/CdS Quantum-Dot Quantum-Well Heterostructures. Nano Lett.* 2006**, 6**, 1940-1949.

[55] B. G. Jeong, Y.-S. Park, J. H. Chang, I. Cho, J. K. Kim, H. Kim, K. Char, J. Cho, V. I. Klimov, P. Park, D. C. Lee, W. K. Bae, *Colloidal Spherical Quantum Wells with Near-Unity Photoluminescence Quantum Yield and Suppressed Blinking. ACS Nano.* 2016, **10**, 9297-9305.

[56] J. Xu, D. Battaglia, X. Peng, M. Xiao, *Photoluminescence from colloidal CdS-CdSe-CdS quantum wells. J. Opt. Soc. Am. B.* 2005, **22**, 1112-1116.

[57] M. Braun, C. Burda, M. A. El-Sayed, *Variation of the Thickness and Number of Wells in the CdS/HgS/CdS Quantum Dot Quantum Well System. J. Phys. Chem. A.* 2001**, 105**, 5548-5551.

[58] J. Cassidy, M. Zamkov, *Nanoshell Quantum Dots: Quantum Confinement Beyond the Exciton Bohr Radius. J. Chem. Phys.* 2020, **152**, 110902.

[59] N. Razgoniaeva, M. Yang, P. Garrett, N. Kholmicheva, P. Moroz, H. Eckard, L. Royo Romero, D. Porotnikov, D. Khon, M. Zamkov, *Just Add Ligands: Self-Sustained Size Focusing of Colloidal Semiconductor Nanocrystals. Chem. Mater.* 2018*,* **30**, 1391-1398.

[60] N. Kholmicheva, M. Yang, P. Moroz, H. Eckard, A. Vore, J. Cassidy, M. Pushina, A. Boddy, D. Porotnikov, P. Anzenbacher, M. Zamkov, *Ion-Mediated Ligand Exchange and Size-Focusing Of Semiconductor Nanocrystals in Ligand-Saturated Solutions. J. Phys. Chem. C* 2018*,* **122**, 23623-23630.

[61] A. F. Cihan, Y. Kelestemur, B. Guzelturk, O. Yerli, U. Kurum, H. G. Yaglioglu, A. Elmali, H. V. Demir, *Attractive versus Repulsive Excitonic Interactions of Colloidal Quantum Dots Control Blue- to Red-Shifting (and Non-shifting) Amplified Spontaneous Emission*. *J. Phys. Chem. Lett.* 2013*,* **4**, 4146-4152.

[62] T. Aimono, Y. Kawamura, K. Goushi, H. Yamamoto, H. Sasabe, C. Adachi, *100% fluorescence efficiency of 4,4'-bis[(N-carbazole)styryl]biphenyl in a solid film and the very low amplified spontaneous emission threshold. Appl. Phys. Lett.* 2005*,* **86**, 071110.

[63] P. J. A. Thijs, L. F. Tiemeijer, P. I. Kuindersma, J. J. M. Binsma, T. Van Dongen, *High-performance 1.5 μm wavelength InGaAs-InGaAsP strained quantum well lasers and amplifiers. IEEE J. Quantum Electron.* 1991, **27**, 1426−1439.

[64] Y. Kelestemur, D. Dede, K. Gungor, C. F. Usanmaz, O. Erdem, H. V. Demir, *Alloyed Heterostructures of $CdSe_xS_{1-x}$ Nanoplatelets with Highly Tunable Optical Gain Performance. Chem. Mater.* 2017, **29**, 4857−4865.

[65] Y. Altintas, U. Quliyeva, K. Gungor, O. Erdem, Y. Kelestemur, E. Mutlugun, M. V. Kovalenko, H. V. Demir, *Highly Stable, Near-Unity Efficiency Atomically Flat Semiconductor Nanocrystals of CdSe/ZnS Hetero-Nanoplatelets Enabled by ZnS-Shell Hot-Injection Growth. Small* 2019, **15**, 1804854.

[66] Q. Li, Z. Xu, J. R. McBride, T. Lian, *Low Threshold Multiexciton Optical Gain in Colloidal CdSe/CdTe Core/Crown Type-II Nanoplatelet Heterostructures. ACS Nano.*2017, **11**, 2545−2553.

[67] Y. Wang, K. E. Fong, S. Yang, V. D. Ta, Y. Gao, Z. Wang, V. Nalla, H. V. Demir, H. Sun, *Unraveling the ultralow threshold stimulated emission from CdZnS/ZnS quantum dot and enabling high-Q microlasers. Laser Photon. Rev.* 2015, **9**, 507–516.

[68] C. Dang, J. Lee, C. Breen, J. S. Steckel, S. Coe-Sullivan, A. Nurmikko, *Red, green and blue lasing enabled by single-exciton gain in colloidal quantum dot films. Nat. Nanotechnol.* 2012, **7**, 335-339.

[69] L. T. Kunneman, M. Zanella, L. Manna, L. D. A. Siebbeles, J. M. Schins, *Mobility and Spatial Distribution of Photoexcited Electrons in CdSe/CdS Nanorods. J. Phys. Chem. C* 2013, **117**, 3146-3151.

[70] M. G. Lupo, F. D. Sala, L. Carbone, M. Zavelani-Rossi, A. Fiore, L. Lüer, D. Polli, R. Cingolani, L. Manna, G. Lanzani, *Ultrafast Electron−Hole Dynamics in Core/Shell CdSe/CdS Dot/Rod Nanocrystals*. *Nano Lett.* 2008, **8**, 4582-4587.

[71] E. R. Smith, J. M. Luther, J. C. Johnson, *Ultrafast Electronic Delocalization in CdSe/CdS Quantum Rod Heterostructures*. *Nano Lett.* 2011, **11**, 4923-4931.

[72] J. M. Pietryga, K. K. Zhuravlev, M. Whitehead, V. I. Klimov, R. D. Schaller, *Evidence for Barrierless Auger Recombination in PbSe Nanocrystals: A Pressure-Dependent Study of Transient Optical Absorption. Phys. Rev. Lett.* 2008, **101**, 217401.

[73] L. W. Wang, M. Califano, A. Zunger, A. Franceschetti, *Pseudopotential Theory of Auger Processes in CdSe Quantum Dots. Phys. Rev. Lett.* 2003, **91**, 056404.

[74] J. J. Li, Y. A. Wang, W. Guo, J. C. Keay, T. D. Mishima, M. B. Johnson, X. Peng, *Large-Scale Synthesis of Nearly Monodisperse CdSe/CdS Core/Shell Nanocrystals Using Air-Stable Reagents via Successive Ion Layer Adsorption and Reaction. J. Am. Chem. Soc.* 2003, **125**, 12567-12575.

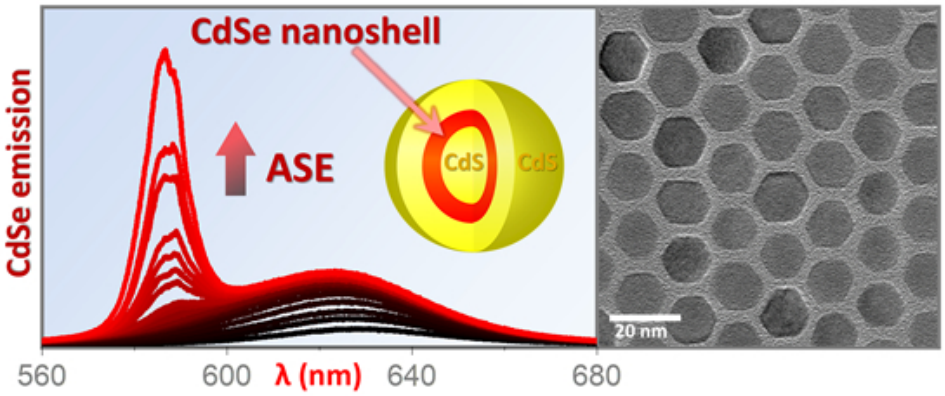

152x60mm (96 x 96 DPI)